An Interpretive Basis of the Proton Nuclear Magnetic Resonance Hyperfine Shifts for Structure Determination of High-Spin Ferric Hemoproteins. Implications for the Reversible Thermal Unfolding of Ferricytochrome *c*′ from *Rhodopseudomonas palustris*

Kimber Clark,[†] Laxmichand B. Dugad,[†] Robert G. Bartsch,[‡] Michael A. Cusanovich,[‡] and Gerd N. La Mar*,[†]

Contribution from the Department of Chemistry, University of California, Davis, California 95616, and Department of Biochemistry, University of Arizona, Tucson, Arizona 85721

Received November 3, 1995[⊗]

Abstract: An NMR approach to determining the solution molecular structure of a high-spin ferric hemoprotein, 13 kDa ferricytochrome *c*′ from *Rhodopseudomonas palustris* (*Rp*), has been investigated. In parallel with the use of appropriately tailored 1D and 2D experiments to provide scalar and dipolar correlations for the strongly relaxed and hyperfine-shifted heme cavity residues, we explore an interpretive basis of the large hyperfine shifts for noncoordinated residues which could provide constraints in solution structure determination for high-spin ferric hemoproteins. It is shown that the complete heme can be uniquely assigned in spite of the extreme relaxation properties (T_1s 1−8 ms). Sufficient scalar connectivities are detected for strongly relaxed protons ($T_1 \geq 4$ ms) to uniquely assign residues on both the proximal and distal sides of the heme. The spatial correlations indicate that the structure is homologous to the four-helix bundle observed for other cytochromes *c*′. The pattern of large hyperfine shifts for noncoordinated residues is shown to be qualitatively reproduced by the dipolar shifts for a structural homolog based on an axial zero-field splitting of ∼12 cm^{-1}. It is concluded that, when this approach is combined with more conventional 2D methods for the diamagnetic portion of the protein, a complete structure determination of a five-coordinate ferric hemoprotein should be readily attainable. It is shown that the ferricytochrome c′ unfolds reversibly at high temperature and that there exists at least one equilibrium intermediate in this unfolding that is suggested to involve helix separation from the heme.

Introduction

Cytochrome *c*′, found in photosynthetic bacteria, is a member of the family of electron transfer proteins where the heme (heme *c*) is covalently bound to the peptide via thioether linkages to the Cys in the consensus sequence Cys-X-Y-Cys-His, with the His serving as the proximal axial ligand,[1,2] as shown in Figure 1. In contrast to the monomeric mitochondrial cytochromes *c*, where the linkage occurs near the N-terminus and which invariably are low-spin due to the distal ligation of Met, the usually dimeric cytochromes *c*′ have the linkage near the C-terminus and the iron is five-coordinate and, hence, predominately high-spin in both oxidation states.[3,4] The unusually low affinity for exogenous strong field ligands,[2,5] the variable cooperativity among different genetic variants,[6] a p*K* in the physiological range that alters the redox properties,[7] and the unusual proposed $S = {}^5/_2, {}^3/_2$ spin-admixed ground state[8,9] have focused interest on the molecular structure of cytochromes *c*′. Crystal structures have been reported for *Chromatium vinosum* (*Cv*),[10,11] *Rhodospirillum molischianum* (*Rm*),[12,13] and *Rho-*

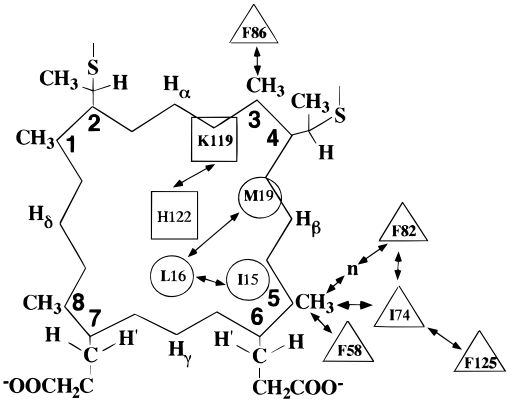

Figure 1. Schematic representation of the heme pocket structure of *Rp* ferricytochrome *c*′. The general positions of the proximal (squares), distal (circles), and peripheral (triangles) residues assigned herein are placed in accordance with the *Rm* cytochrome c′ crystal structure. Observed NOE connectivities are designated by arrows.

[†] University of California.
[‡] University of Arizona.
[⊗] Abstract published in *Advance ACS Abstracts,* April 15, 1996.

(1) Ambler, R. P. *The Evolution of Metalloenzymes, Metalloproteins and Related Materials*; Ambler, R. P., Ed.; Symposium Press: London, 1977; pp 100−118.
(2) Bartsch, R. G. *The Photosynthetic Bacteria*; Clayton, R. K., Sistrom, W. R., Eds.; Plenum Press: New York, NY, 1978; pp 249−279.
(3) Cusanovich, M. A.; Meyer, T. E.; Tollin, G. *Advances in Inorganic Biochemistry: Heme Proteins*; Eichhorn, G. L., Marjilla, L. G., Eds.; Elsevier: New York, 1988; pp 37−91.
(4) Meyer, T. E.; Kamen, M. D. *Adv. Protein Chem.* **1982**, *35*, 105−212.
(5) Kassner, R. J.; Kykta, M. G.; Cusanovich, M. A. *Biochim. Biophys. Acta* **1985**, *831*, 155−158.
(6) Kassner, R. J. *Biochim. Biophys. Acta* **1991**, *1058*, 8−12.
(7) Barakat, R.; Strekas, T. C. *Biochim. Biophys. Acta* **1982**, *679*, 393−399.
(8) Weber, P. C.; Bartsch, R. G.; Cusanovich, M. A.; Hamlin, R. C.; Howard, A.; Jordan, S. R.; Kamen, M. D.; Meyer, T. E.; Weatherford, D. W.; Xuong, N. H.; Salemme, F. R. *Nature* **1980**, *286*, 302−304.
(9) Maltempo, M. M. *Q. Rev. Biophys.* **1976**, *9*, 181−215.

S0002-7863(95)03719-X CCC: $12.00

dospirillum rubrum (*Rr*)[14] cytochromes *c*′ which reveal similar dimeric structures with each polypeptide monomer folding into a four-helical bundle similar to that exhibited by cytochrome b_{562}[15] and the tobacco mosaic virus coat protein,[16] among others. The four-helical bundle presents an interesting structural motif for the investigation of the mechanism of protein folding, and many synthetic versions of this type of protein have been reported.[17] A recent solution NMR study of ^{15}N,^{13}C-labeled dimeric ferricytochrome *c*′ from *Rhodobacter capsulatus* (*Rc*)[18] has provided assignments and structural information for the "diamagnetic" portion of the protein; resonances not detected were those which are expected to be closer to the iron than 9 Å.

Cytochrome *c*′ from *Rhodopseudomonas palustris* (*Rp*) exhibits extensive sequence and functional homology to the structurally characterized dimeric cytochromes *c*′, but differs in that it is exclusively monomeric in solution.[2] ^{1}H NMR investigations[19−24] of several ferricytochromes *c*′ have supported the deprotonation of the axial His in the characteristic acid → alkaline transition,[19,25] but have been interpreted[22] in terms of $S = {}^5/_2$, rather than a spin-admixed[9] ground state for the acidic form. The ^{1}H NMR analysis was based on the pattern of heme methyl versus meso-H hyperfine shifts for which assignment was based solely on the comparison to model compounds.[26] The early ^{1}H NMR studies[20,22] also indicated some inflections in spectral parameters at high temperature that suggested structural changes. However, identification of the spin ground state and interpretation of the nature of structural changes first require the definitive assignment of the residues in the heme cavity, including the heme, and determination of the structure of the protein. Both exercises provide a challenge for ^{1}H NMR because of the strongly paramagnetic center that results in broad signals, spectral overlap, and enhanced spin−lattice relaxation,[27] as given by $T_1^{-1} = \gamma^2 g^2 \beta^2 S(S+1) R_{Fe}^{-6} f(T_{1e})$, where R_{Fe} is the distance from the iron and T_{1e} is the electronic spin−lattice relaxation time. For nonequivalent protons *i*, *j*, this leads to

$$T_{1i}/T_{1j} = R^6_{Fe-i}/R^6_{Fe-j} \quad (1)$$

For the ligated heme and axial His, the paramagnetism also leads to significant contact shifts given by[28]

$$\delta_{con} = (A/\hbar)\frac{g\beta S(S+1)}{3\gamma_n kT} \quad (2)$$

where $A/\hbar$ is proportional to the delocalized spin density on the nucleus. For an α-methylene group on the heme, *A* is dependent on the H−C_α−C_π angle, ψ, with the heme normal,[29] *i.e.*,

$$A = B\cos^2\psi \quad (3)$$

The dipolar shift for an axially symmetric high-spin ferric system is given by[28]

$$\delta_{dip} = \frac{-28g^2\beta^2}{9k^2T^2}\left[\frac{3\cos^2\theta - 1}{R_{Fe^3}}\right]D \quad (4)$$

where *D* is the zero-field splitting constant and θ is the angle between the Fe−proton vector and the heme normal. It is noted that, for $S = {}^5/_2$ iron, the contact shift exhibits T^{-1}, while the dipolar shift exhibits T^{-2} temperature dependence.[28] Thus hyperfine shifts can provide resolution in spite of line broadening by expanding the ^{1}H chemical shift scale of the active site by $\sim 10^2$ over a similar diamagnetic system. The ability to assign resonances and determine the solution structure of a paramagnetic protein depends on a large ratio of the shift dispersion to the line broadening. T_1, δ_{con}, and δ_{dip}, in addition to providing insight into the electronic structure, provide unique molecular and structural information[30] in R_{Fe}, ψ, and θ in eqs 1−4, *if the resonances can be assigned*.

Recent studies have shown that molecular structure determination of paramagnetic metalloproteins is possible by adapting the conventional 2D NMR methods for detecting relaxed and shifted proton signals.[31] For low-spin iron(III) such as in ferricytochromes *c*[32] and *b*[33] and cyano-met myoglobins,[34] complete assignment and spatial localization of the paramagnetically influenced protons in the heme cavity have been achieved, with the remainder of the protons addressable by conventional 2D methods. Moreover, it has been shown that, while certain conventional NOE information near the paramagnetic center may be lost due to enhanced relaxation, the δ_{dip}

(10) Abbreviations used: *Chromatium vinosum*, *Cv*; *Rhodospirillum rubrum*, *Rr*; *Rhodospirillum molischianum*, *Rm*; *Rhodobacter capsulatus*, *Rc*; *Rhodopseudomonas palustris*, *Rp*.

(11) Ren, Z.; Meyer, T.; McRee, D. E. *J. Mol. Biol.* **1993**, *234*, 433−445.
(12) Weber, P. C.; Howard, A.; Nguyen, H. X.; Salemme, F. R. *J. Mol. Biol.* **1981**, *153*, 399−424.
(13) Weber, P. C.; Bartsch, R. G.; Cusanovich, R. C.; Hamlin, A.; Howard, S. R.; Jordan, M. D.; Kamen, M. D.; Meyer, T. E.; Weatherford, D. W.; Nguyen, H. X.; Salemme, F. R. *Nature* **1980**, *286*, 302−304.
(14) Yasui, M.; Harada, S.; Kai, Y.; Kasai, N.; Kusunoki, M.; Matsuura, Y. *J. Biochem.* **1992**, *111*, 317−324.
(15) Xavier, A. V.; Czerwinski, E. W.; Bethge, P. H.; Mathews, F. S. *Nature* **1978**, *275*, 245−247.
(16) Amalric, J. C.; Merkel, C.; Gelfand, R.; Attardi, G. J. *J. Mol. Biol.* **1978**, *118*, 1−25.
(17) Ho, S. W.; DeGrado, W. F. *J. Am. Chem. Soc.* **1987**, *109*, 6751−6758. Regan, L.; DeGrado, W. F. *Science* **1988**, *241*, 976−978. DeGrado, W. F.; Wasserman, Z. R.; Lear, J. D. *Science* **1989**, *1989*, 622−628.
(18) Caffrey, M.; Simorre, J.-P.; Brutscher, B.; Cusanovich, M.; Marion, D. *Biochemistry* **1995**, *34*, 5904−5912.
(19) Emptage, M. H.; Xavier, A. V.; Wood, J. M.; Alsaadi, B. M.; Moore, G. R.; Pitt, R. C.; Williams, R. J. P.; Ambler, R. P.; Bartsch, R. G. *Biochemistry* **1981**, *20*, 58−64.
(20) Jackson, J. T.; La Mar, G. N.; Bartsch, R. G. *J. Biol. Chem.* **1983**, *258*, 1799−1805.
(21) Akutsu, H.; Kyogoku, Y.; Horio, T. *Biochemistry* **1983**, *22*, 2055−2063.
(22) La Mar, G. N.; Jackson, J. T.; Dugad, L. B.; Cusanovich, M. A.; Bartsch, R. G. *J. Biol. Chem.* **1990**, *265*, 16173−16180.
(23) Banci, L.; Bertini, I.; Turano, P.; Vincens Oliver, M. *Eur. J. Biochem.* **1992**, *204*, 107−112.
(24) Bertini, I.; Gori, G.; Luchinat, C.; Vila, A. J. *Biochemistry* **1993**, *32*, 776−783.
(25) Weber, P. C. *Biochemistry* **1982**, *21*, 5116−5119.
(26) La Mar, G. N.; Walker, F. A. *The Porphyrins*; Dolphin, D., Ed.; Academic Press: New York, 1978; Vol. IV, pp 61−157. Walker, F. A.; Simonis, U. *Biol. Magn. Reson.* **1993**, *12*, 133−274.
(27) Swift, T. In *NMR of Paramagnetic Molecules*; La Mar, G., Horrocks, W. D., Jr., Holm, R. H., Eds. Academic Press: New York, 1973; pp 52−85. Bertini, I.; Luchinat, C. *NMR of Paramagnetic Molecules in Biological Systems*; Benjamin/Cummings: Menlo Park, CA, 1986; pp 47−57.
(28) Kurland, R. J.; McGarvey, B. R. *J. Magn. Reson.* **1970**, *2*, 286−301.
(29) La Mar, G. N. In *NMR of Paramagnetic Molecules*; La Mar, G., Horrocks, W. D., Jr., W. D.; Holm, R. H., Eds.; Academic Press: New York, 1973; pp 52−86.
(30) Bertini, I.; Turano, P.; Vila, A. J. *Chem. Rev.* **1993**, *93*, 2833−2932.
(31) La Mar, G. N.; de Ropp, J. S. *Biol. Magn. Reson.* **1993**; *18*, 1−78.
(32) Williams, G.; Clayden, N. J.; Moore, G. R.; Williams, R. J. P. *J. Mol. Biol.* **1985**, *183*, 447−460. Feng, Y.; Roder, H.; Englander, S. W. *Biochemistry* **1990**, *29*, 3494−3504.
(33) Veitch, N. C.; Concar, D. W.; Williams, R. J. P.; Whitford, D. *FEBS Lett.* **1988**, *238*, 49−55. Guiles, R. D.; Basus, V.; Kuntz, I. D.; Waskell, L. *Biochemistry* **1992**, *31*, 11365−11375.
(34) Emerson, S. D.; La Mar, G. N. *Biochemistry* **1990**, *29*, 1545−1555; Rajarathnam, K.; Qin, J.; La Mar, G. N.; Chiu, M. L.; Sligar, S. G. *Biochemistry* **1993**, *32*, 5670−5680. Qin, J.; La Mar, G. N.; Travaglini Allocatelli, C.; Brancaccio, A. *Biophys. J.* **1993**, *65*, 2178−2190.

Table 1. Residues in *Rm* Cytochrome *c′* with a Proton ≤9 Å from the Iron and the Equivalent Residues in *Rp* Cytochrome *c′* [a,b]

	12	13	**15**	**16**	17	**19**	20	**54**	**58**	82	**86**	**89**	**118**	**119**	**121**	**122**	125	**126**	*36*	*75*
Rm	R	R	**L**	**M**	Q	**L**	K	**A**	**W**	F	**W**	**L**	**C**	**K**	**C**	**H**	F	**R**	*L*	*F*
Rp	R	K	**I**	**L**	K	**M**	G	**K**	**F**	F	**F**	**L**	**C**	**K**	**C**	**H**	F	**K**	*F*	*W*

[a] Boldface type denotes residues with proton(s) having $R_{Fe} \leq 7.5$ Å. [b] Italics type denote residues with proton(s) having $R_{Fe} \geq 10$ Å.

and/or T_1s provide significant constraints in developing robust structural models.[34−36] In this report we address the feasibility for determining the solution structure of the 13 kDa *Rp* ferricytochrome *c′* which exhibits line widths and T_1^{-1} an order of magnitude greater than the low-spin hemoproteins addressed previously.[32−34] Our goal here is not to determine the structure at this time, but to (1) assign the heme signals; (2) identify and spatially locate the strongly relaxed residues in the cavity relative to each other and the heme; (3) determine the qualitative validity of an interpretive basis of both eqs 2 and 3 for providing structural information from hyperfine shifts; and (4) assess the utility of the exquisite sensitivity of hyperfine shifts to environment in providing information on the mechanism of unfolding of the protein. It is clear that, if the resonances closest to the iron yield to these specific goals, the remainder of the "diamagnetic" protein can be addressed by 2D NMR methods[18] common to wholly diamagnetic proteins of comparable size.

Experimental Section

Sample Preparation. *Rp* ferricytochrome *c′* was isolated and purified according to well-established methods.[2,37] The NMR samples were ca. 9 mM in concentration and were prepared by dissolving the protein in 99.8% ^2H_2O without buffer, followed by the removal of particulate matter via centrifugation. The solution pH was adjusted using ^{2}HCl or NaO^{2}H, and the pH values were monitored using a Beckman (Model 3500) pH meter. The reported pH values were not corrected for the isotope effect.

Homology Model. A qualitative homology model for *Rp* ferricytochrome *c′* was constructed by substituting the residues which have a proton within 9 Å of the iron in a reference ferricytochrome *c′* by the appropriate *Rp* residue. The closest sequence homology to *Rp* ferricytochrome *c′* is found in *Rm* ferricytochrome *c′*, which serves as reference protein.[12,13] In all but two cases (*Rm* Ala54, Lys25 → *Rp* Lys, Gly), the substitutions are quite conservative, and adjusting the side chain bond angles avoided any violation of the van der Waals surfaces without resorting to energy minimization. The substituted residues are shown in Table 1; also included in Table 1 in italics are the two aromatic side chains in *Rp* (Phe36, Trp75) which are remote from the heme. The residues with a proton with $R_{Fe} \leq 7.5$ Å are given in bold in Table 1 and include residues on helix 1 (Ile15, Leu16, and Met19), the loop connecting helix 2 and helix 3 (Lys54 and Phe58), helix 3 (Phe86 and Leu89), and helix 4 (Cys118, Lys119, Cys121, His122, and Lys126). While high structural homology is generally observed for the heme region for the structurally characterized[11−14] cytochromes *c′*, poor conservation is noted in the region containing the connecting loops between helix 2 and helix 3 which exhibit significant variations in the peptide backbone and amino acid side chain location relative to the heme.

NMR Data Collection. The 360 and 500 MHz ^{1}H NMR spectra of the acidic and alkaline forms of the *Rp* ferricytochrome *c′* were obtained over the temperature range 5−85 °C on Nicolet 360 and GE Ω-500 spectrometers, respectively. Using a spectral width of 90.9 kHz, spectra were collected by the normal one-pulse sequence with ^1H_2O presaturation using either a slow (3 s) recycle time, τ_{rec}, or a fast (0.1 s) τ_{rec}, or with the WEFT pulse sequence[38] using τ_{rec} of 0.05−0.25 s and a relaxation delay, τ_{rd}, of 20−100 ms. Nonselective spin−lattice relaxation times, T_1, were collected using an inversion−recovery pulse sequence with a recycle time of 5 times the T_1 of the peak(s) of interest. T_1 values were determined from the initial slope of the magnetization recovery data for resolved peaks (uncertainties ±15%) or estimated from the null point for partially resolved peaks (uncertainty ±50%). Steady-state nuclear Overhauser effect, NOE, spectra were collected as described previously[39] using a low-power decoupler pulse sufficient to saturate the peak of interest by ∼30% for ∼30 ms.

The 2D ^{1}H NMR experiments were performed at 500 MHz using 512 t_1 blocks of 2048 t_2 complex points, except where noted. The WEFT-NOESY[40] spectrum was collected at 45 °C using a $\tau_{rec}$of ∼90 ms, a τ_{rd} of ∼30 ms after the initial 180 ° pulse, and a mixing time, τ_m, of 6 ms. A 100 kHz spectral width was employed with 1344 scans per block. Additional phase-sensitive NOESY[41] spectra were acquired at 30 and 40 °C over spectral widths of 6.0 and 8.0 KHz, respectively, and using τ_{rec} between 0.2 and 2 s and τ_m of 15, 50, and 150 ms. TOCSY[42] spectra were recorded at 30 and 40 °C over spin lock fields of 6.0 and 8.0 kHz, respectively, using spin lock times of 22 ms (for optimal detection of three-bond *J* coupling for only weakly relaxed times) (1024 t_1 complex points) and 8 ms (an effective compromise between incompletely developed coherence for three-bond *J* coupling and coherence decay due to significant line broadening by the iron paramagnetism) for τ_{rec} of 1.6 s and 160 ms, respectively.

NMR Data Processing. The 500 MHz reference spectra were subjected to 10 Hz exponential apodization to increase signal-to-noise and emphasize fast-relaxing resonances. NMR data sets were transferred to a Sun Sparkstation and processed using the General Electric Omega software package. For WEFT-NOESY, a 60°-shifted sine-bell-squared apodization was applied over 251 and 1024 points in t_1 and t_2, respectively. Both dimensions were phase corrected, base-line straightened, and zero-filled to 2048 × 2048 points prior to Fourier transformation. The remaining 2D data were transferred to a Silicon Graphics Indigo computer and processed using the Felix 2.3 software package. Data were processed using either a 30°- or a 60°-shifted sine-bell-squared apodization applied over 512 t_1 and 2048 t_2 and 256 t_1 and 1024 t_2 points, respectively.

The observed chemical shift (δ_{DSS}), indirectly referenced to 2,2-dimethyl-2-silapentane-5-sulfonate (DSS) via the solvent signal, is composed of diamagnetic (δ_{dia}), contact (δ_{con}), and dipolar (δ_{dip}) contributions:

$$\delta_{DSS} = \delta_{dia} + \delta_{con} + \delta_{dip} \quad (5)$$

The diamagnetic term is that which is observed for an analogous diamagnetic protein; this can be calculated if the molecular structure is known. Experimentally, δ_{dia} is given by the intercept at $T = \infty$ (δ_{int}) of the appropriate temperature-dependent plots, $\delta_{int}(T^{-1})$ for δ_{con} and $\delta_{int}(T^{-2})$ for δ_{dip}. For noncoordinated residues, the δ_{con} is 0 and the observed δ_{dip} can be expressed as

$$\delta_{dip}(\text{obsd}) = \delta_{DSS}(\text{obsd}) - \delta_{dia} \quad (6)$$

Results

Strategy. A recent 2D ^{1}H/^{15}N NMR study[18] on *Rc* ferricytochrome *c′* has shown that conventional 2D NMR strategy in a ^{15}N-labeled protein allows assignments and structure determination outside a 9 Å sphere of the iron, for which $T_1 \geq 100$ ms. Our goal here is to address solely the protons on residues

(35) Harper, L. V.; Amann, B. T.; Vinson, V. K.; Berg, J. M. *J. Am. Chem. Soc.* **1993**, *115*, 2577−2580.
(36) Gochin, M.; Roder, H. *Protein Sci.* **1995**, *4*, 296−305.
(37) Bartsch, R. G. *Methods Enzymol.* **1971**, *23*, 344−363.
(38) Gupta, R. K. *J. Magn. Reson.* **1976**, *24*, 461−465.
(39) Thanabal, V.; de Ropp, J. S.; La Mar, G. N. *J. Am. Chem. Soc.* **1987**, *109*, 265−272.
(40) Lankhorst, P. P.; Wille, G.; Van Boom, J. H.; Altona, C.; Haasnoot, C. A. G. *Nucleic Acids Res.* **1983**, *11*, 2839−2856.
(41) Jeener, B. H.; Meier, P.; Bachman, P.; Ernst, R. R. *J. Chem. Phys.* **1975**, *71*, 4546−4553.
(42) Bax, A.; Davis, D. G. *J. Magn. Reson.* **1985**, *65*, 355−260. Cavanagh, J.; Rance, M. *J. Magn. Reson.* **1990**, *88*, 72−85.

Table 2. ^{1}H NMR Spectral Parameters for Heme and Axial His Resonances for *Rp* Ferricytochrome *c*′ in ^2H_2O, pH 5.0 at 40 °C

peak label[a]	assignment	δ_{DSS}(obsd) (ppm)	T_1 (ms)[b]	δ_{dip}(calcd)[c] (ppm)
h_1	1-CH_3	76.5	8	+8
h_3	3-CH_3	61.6	8	+8
h_5	5-CH_3	68.6	8	+8
h_8	8-CH_3	81.0	8	+8
h_α	α-meso-H	−11.9[d]	∼1[e]	+18
h_β	*β*-meso-H	−26.4	∼1[e]	+18
h_γ	*γ*-meso-H	−16.2[d]	∼1[e]	+18
h_δ	*δ*-meso-H	−21.8	∼1[e]	+18
$h_{2\alpha}$	2-H_α	20.9	4	+8
$h_{2\beta}$	2-$C_\beta H_3$	10.0	14	+4
$h_{4\alpha}$	4-H_α	49.3	5	+6
$h_{4\beta}$	4-$C_\beta H_3$	5.8	*f*	+4
$h_{6\alpha}$	6-H_α	43.4	9	+6
$h_{6\alpha'}$	6-$H_{\alpha'}$	42.1	6	+8
$h_{6\beta}$	6-H_β	6.9	*f*	+4
$h_{6\beta'}$	6-$H_{\beta'}$	3.4	*f*	+4
$h_{7\alpha}$	7-$H_{\alpha'}$	45.7	8	+6
$h_{7\alpha'}$	6-H_α	47.2	6	+8
H_1	His122 H_β	37.4	3	−12
H_2	His122 $H_{\beta'}$	36.6	3	−12

[a] Labeled as shown in Figures 2 and 6. [b] T_1 values from inversion recovery experiment, ±15%. [c] From eq 4 with $D = 12$ cm^{-1} and coordinates from the homology model. [d] Peak is not resolved at 40 °C. δ_{DSS}(obsd) at 40 °C is calculated from the extrapolated temperature dependence in Figure 5. [e] Estimated from null point. [f] Peak is under the diamagnetic envelope.

well within this sphere, $R_{Fe} = 7.5$ Å, with target T_1s ≤30 ms, emphasizing those protons closest to the iron, starting with the heme. Our protocol for obtaining assignments and determining the structure of the heme cavity relies on a combination of conventional 2D NMR, TOCSY optimized for short T_2 to detect scalar, and NOESY optimized to detect spatial (dipolar) correlations.[31] These methods are augmented by the use of steady-state NOEs involving resonances with extreme relaxation times (≤2 ms), and differential dipolar relaxation (eq 4) to determine distances to the iron (R_{Fe}) with a heme methyl at $R_{Fe} = 6.1$ Å as standard.[43] Lastly, we make the reasonable assumption that the structure of *Rp* ferricytochrome *c*′ is homologous to that of the structurally characterized dimeric analogs, which are very similar to each other,[11−14,18] and that dipolar shifts are given[28] by eq 4 with $D \sim 12$ cm^{-1}. These latter two assumptions are not necessary to make the assignments and, in fact, can be deduced from the NMR spectral parameters. These assumptions, however, will greatly expedite the assignment/structural protocol. The validity of these assumptions will be addressed later.

Homology Model Predictions. The pattern of dipolar shifts expected[28,44,45] for a positive *D* for an axial system is upfield shifts for protons near the heme normal ($\theta < 54°$ in eq 4) and downfield shifts for protons near the heme periphery ($\theta > 54°$ in eq 4). For the heme protons, $\theta = 90°$ in eq 4 and all dipolar shifts are to low field (Table 2). Nonligated residues expected to exhibit solely upfield and sizable (≥5 ppm) dipolar shifts are Ile15, Leu16, Met19, and Lys119; Phe82 and Phe125 predict upfield but only minor δ_{dip} (≤3 ppm) (Table 3). Solely downfield and large (≥4 ppm) dipolar shifts are predicted only for protons on Cys118, Cys121, and Phe82 (Table 3); Lys17, Gly20, Leu89, and Phe125 exhibit only low-field but small δ_{dip} (supporting information; Table 2S). Phe36 and Trp75 are not expected to exhibit significant δ_{dip}. The remainder of the residues in Table 1 lie close to or across the nodal surface (*i.e.*, $\theta \sim 54°$ in eq 4) of the dipolar field and exhibit both up- and downfield δ_{dip}. However, only Lys126 is close enough to the iron to exhibit large δ_{dip} in both directions (Tables 2S, 3). Other residues in this category exhibit small shifts in both directions (supporting information; Table 2S). Hence the homology model is likely to be least reliable for predicting the shift magnitude/direction for residues near this nodal surface.

The R_{Fe} and δ_{dip}(calcd) predicted for our target residues in the homology model of *Rp* ferricytochrome *c*′ are listed in Table 2 for select heme and His122 protons, and in Table 3 for nonligated residues which give rise to resolved and/or assignable proton peaks. The observed T_1s are converted[43] to R_{Fe} via eq 1 using the observed heme methyl $T_1 = 8$ ms and $R_{Fe} = 6.1$ Å. The primary residues of interest with $R_{Fe} \leq 7.5$ Å (bold in Table 1) convert to $T_1 \leq 30$ ms. Similar information on residues in Table 3 that are not assigned is given in supporting information, Table 2S.

^{1}H NMR Spectral Parameters. A total of 39 signals exhibit strong relaxation effects ($T_1 \leq 50$ ms) and are resolved at some temperatures 10−70 °C within the 90 to −40 ppm window. All resonances relevant to this study are labeled by a symbol that is related to its ultimate assignment (if attainable) as follows: h_i for heme protons where $i = 1-8$ for the pyrroles and $i = \alpha-\delta$ for the four meso-H atoms (Figure 1); protons arising from an amino acid are labeled X_i, where X is the standard upper-case one-letter code for the amino acid to which we can make assignment, and *i* is an integer from one through the number of peaks assigned for that residue, in order of decreasing dipolar shift; resonances which cannot be assigned to a type of amino acid are labeled by lower-case letters, x_i, where *i* is the index for the number of the located protons for this residue.

The resolved portions of the 360 MHz ^{1}H NMR spectra downfield of 15 ppm of *Rp* ferricytochrome *c*′, pH 5.0, at several temperatures are shown in Figure 2 and consist of 13 resolved resonances, four with three-proton intensity (h_1, h_3, h_5, h_8) and nine with single-proton intensity. This region of the spectrum is similar to that of other ferricytochromes *c*′,[19−25] except that *Rp* exhibits one more single-proton peak in the low-field spectra. The resonances move upfield with increasing temperature. Above 80 °C, the set of resonances h_i lose intensity and a new species with three broad resonances, labeled u_1, u_2, and u_3 with relative intensity ∼6:3:2, appears and becomes dominant at 83 °C (Figure 2D). The loss of all structural features in the diamagnetic envelope upon raising the temperature above 80 °C, as shown in Figure 3, indicates that the species responsible for peaks u_1, u_2, and u_3 is unfolded; the process is completely reversible.

All ferricytochromes *c*′ undergo an acid ⇔ alkaline transition[7,8,19−25] marked by significant (∼10 ppm) shift changes in the low-field window. The pH profiles for peak h_8 at 25 and 55 °C are shown in Figure 4 and indicate that temperature changes at pH 5 reflect solely changes in the properties of a single species, namely, the acidic form of the protein. The temperature dependent spectra for the alkaline species at pH 10 are provided as supporting information, Figures 1S and 2S. The chemical shifts for h_i at pH 5.0 and 40 °C are given in Table 2. The temperature dependence for these signals is shown in the form of a Curie plot (plot of δ_{DSS}(obsd) *vs* T^{-1}) in Figure 5. It is noted that, with the exception of peak v, the low-field

(43) The fact that the T_1s for the four heme methyls are the same in spite of their significant differences in contact shift dictates that the relaxation of the heme methyl is insignificantly influenced by delocalized spin density and hence is dominated by dipolar relaxation by the spin density of the iron (Unger, S. W.; Jue, T.; La Mar, G. N. *J. Magn. Reson.* **1985**, *61*, 448−456).

(44) Brackett, G. C.; Richards, P. L.; Caughey, W. S. *J. Chem. Phys.* **1971**, *54*, 4383−4401.

(45) Kao, Y.-H.; Lecomte, J. T. J. *J. Am. Chem. Soc.* **1993**, *115*, 9754−9762.

Table 3. ^{1}H NMR Spectral Parameters for Residues with Resolved Peaks on Nonligated Residues of *Rp* Ferricytochrome *c*′ in ^2H_2O, pH = 5.0 at 40 °C

		Rp ferricytochrome *c*′					homology model		
peak label[a]	assignment	δ_{DSS}(obsd) (ppm)	T_1 (ms)	$\delta_{int}(T^{-1})$[b] (ppm)	$\delta_{int}(T^{-2})$[c] (ppm)	R_{Fe}[d] (Å)	δ_{dip}(obsd) (ppm)[e]	δ_{dip}(calcd) (ppm)	R_{Fe} calcd (Å)
L_1	Leu16 $C_\delta H_3$	−7.57	4	6.9	−0.4	5.4	−7.2	−16	5
L_2	Leu16 $C_{\delta'} H_3$	−4.32	16	3.9	0.5	6.7	−4.8	−2	5
L_3	Leu16 H_β	−2.89	33	*f*	*f*	7.6	*f*	−2	6
L_4	Leu16 H_γ	−2.41	25	3.8	0.7	7.2	−3.1	−5	7
	Leu16 $H_{\beta'}$							−17	4
	Leu16 H_α							−12	5
I_1	Ile15 $C_\gamma H_3$	−2.89	43	3.9	0.5	7.9	−3.4	−5	8
I_2	Ile15 H_β	−2.04	43	5.0	1.5	7.9	−3.5	−3	10
I_3	Ile15 $C_\delta H_3$	−1.15	>100	3.0	1.0	9.4	−2.2	−3	10
I_4	Ile15 H_γ	−0.8	*f*	*f*	*f*	*f*	*f*	−6	8
I_5	Ile15 $H_{\gamma'}$	−0.09	*f*	2.3	1.1	*f*	−1.2	−6	8
I_6	Ile15 H_α	1.38	*f*	6.2	3.8	*f*	−5.2	−3	10
M_1	Met19 $C_\epsilon H_3$	−9.90	<1	10.3	0.3	<4.8	−10.2	−12	5
M_2	Met19 H_γ(?)	−2.9	18	*f*	*f*	6.9	*f*	0	6
M_3	Met19 H_β(?)	−2.3	22	2.6	0.2	7.1	−2.5	−1	7
M_4	Met19 H_α(?)	1.72	*f*	5.4	3.5	*f*	−1.8	−1	9
	Met19 $H_{\beta'}$							−5	6
	Met19 $H_{\gamma'}$							0	8
I_1*	Ile74 $C_\delta H_3$	−0.8	140	−1.6	−1.2	9.7	+0.4	+2	9
I_2*	Ile74 H_γ	1.41	*f*	−0.4	0.5	*f*	+0.9	+2	9
I_3*	Ile74 $H_{\gamma'}$	3.55	*f*	2.0	2.8	*f*	+0.8	+3	11
K_1	Lys119 H_α	−1.50	11	7.8	3.0	6.3	−4.5	−5	7
K_2	Lys119 $H_{\gamma'}$	−0.9	43	4.6	1.7	7.9	−2.6	−2	10
K_3	Lys119 H_γ	−0.6	58	2.7	1.1	8.3	−1.7	−1	11
K_4	Lys119 H_β	−0.2	29	3.4	1.5	7.4	−1.7	−2	9
K_5	Lys119 H_δ	−0.03	*f*	3.0	1.5	*f*	−1.5	−3	9
K_6	Lys119 $H_{\delta'}$	0.07	*f*	1.9	1.0	*f*	−0.9	−3	10
K_7	Lys119 $H_{\beta'}$	0.28	*f*	2.7	1.5	*f*	−1.2	−2	10
K_8	Lys119 H_ϵ	1.64	*f*	3.8	2.7	*f*	−1.1	−1	12
K_9	Lys119 $H_{\epsilon'}$	1.78	*f*	3.6	2.7	*f*	−0.9	−2	12
F_1*	Phe82 *p*-H (?)	8.49	*f*	6.4	7.5	*f*	+1.0	+3	10
F_2*	Phe82 *m*-Hs (?)	7.85	*f*	6.3	7.1	*f*	+0.8	+2[g]	9[g]
F_3*	Phe82 *o*-Hs (?)	7.79	*f*	6.9	7.3	*f*	+0.5	+3[g]	7[g]
	Phe86							−1	7
F_1	Phe86 (?)	6.88	*f*	7.1	7.0	*f*	*f*	−1[g]	8[g]
	Phe86							0[g]	9[g]
$F_{1'}$	Phe125	8.22	*f*	7.3	7.8	*f*	+0.4	+2[g]	10[g]
$F_{2'}$	Phe125	7.69	*f*	5.9	6.8	*f*	+0.9	+1[g]	12[g]
$F_{3'}$	Phe125	7.45	*f*	6.8	7.2	*f*	+0.3	+1	13
$F_{1''}$	Phe36	7.27	*f*	7.0	7.1	*f*	+0.2		
$F_{2''}$	Phe36	7.18	*f*	6.6	6.9	*f*	+0.3		
$F_{3''}$	Phe36	6.94	*f*	6.3	6.6	*f*	+0.3		
F†	Phe58 (?)	7.85	*f*	5.3	6.6	*f*	+1.3	0	10
	Phe58							0	8
	Phe58							+3	7
a	Cys118 H_α	12.4	2	*f*	*f*	4.8	*f*	+6	5
a′	Cys121 H_β	12.2	15	*f*	*f*	6.6	*f*	+4	7
a″	Cys121 $H_{\beta'}$	11.7	5	*f*	*f*	5.5	*f*	+6	5
	Lys126 $H\gamma'$							+4	5
	Lys126 H_δ							−10	5
	Lys126 $H_{\delta'}$							−5	6
q		−16.4	<1	19.4	1.4	<4.8	−17.8		
r		−7.6	2	*f*	*f*	4.8	*f*		
s		−6.0	2	10.1	2.1	4.8	−8.1		
t		−2.9	3	*f*	*f*	5.0	*f*		
z		−1.7	4	*f*	*f*	5.3	*f*		
x	Phe86 (?)	−38.3	<1	60.5	12.8	< 4.8	−51.1	−2	7
v	Lys54 (?)	23.09	2.6	−16.2	4.2	5	+18.9	*h*	*h*

[a] Peak labels are defined in Figures 2 and 6−10. [b] Given by the intercept at $T = \infty$ of the δ_{DDS}(obsd) as a function of T^{-1}. [c] Given by the intercept at $T = \infty$ of the δ_{DDS}(obsd) as a function of T^{-2}. [d] Given by eq 1, using $R_{Fe} = 6.1$ Å for a heme methyl. [e] Given by eq 6, using δ_{dia} given by the intercept of the δ_{DDS}(obsd) as a function of T^{-2}. [f] The peak is not well enough resolved over the temperature range studied to obtain a value for this parameter. [g] The value given is the average of the two equivalent proton groups. [h] Too radical a substitution to predict R_{Fe} or δ_{dip}.

resonances in the Curie plot in Figure 5 exhibit straight lines in the low-temperature limit <50 °C, but show significant curvature above 50 °C. Moreover, one methyl (peak h_1) shows extensive broadening at elevated temperatures (Figure 2C,D). The nonselective T_1s for the resolved low-field resonances at 40 °C are given in Table 2 and are, for the four methyl peaks, indistinguishable, T_1s ∼8 ± 1 ms. The T_1s for the methyl peaks at 60 °C, where h_1 is twice as broad as h_3, h_5, and h_8, are still indistinguishable at 8 ± 1 ms.

Strongly upfield hyperfine shifted and broad resonances are shown in Figure 6A (with peak x better observed in the 60 °C inset A′). Variable temperature spectra (supporting information, Figure 3S) establish the presence of six strongly upfield shifted and strongly relaxed ($T_1 \sim 1$ ms) single-proton signals with

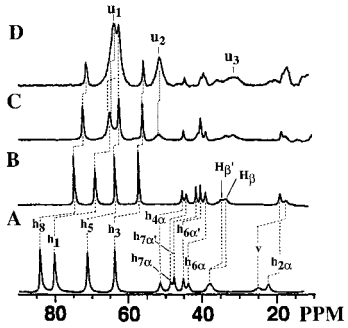

Figure 2. Low-field resolved portions of the 360 MHz ^{1}H NMR spectra of 9 mM *Rp* ferricytochrome *c*′ in ^2H_2O, pH 5.0, at (A) 30 °C; (B) 70 °C; (C) 80 °C; and (D) 83 °C (τ_{rec} = 82 ms). The traces illustrate the broadening of peak h_1 with increasing temperature and the growth of a new species with peaks u_1, u_2, and u_3 at and above 80 °C. Peaks are labeled h_i for the heme with *i* designating the position on the heme as shown in Figure 1; H_β, H_β′ for the axial His122 H_βs; and peak v arising from a nonligated residue.

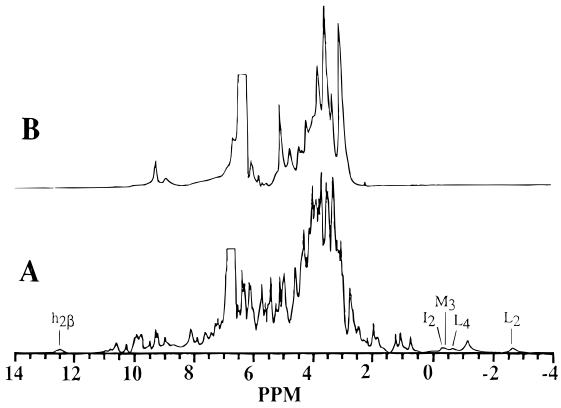

Figure 3. The 14 to −4 ppm window of the 360 MHz ^{1}H NMR spectra of *Rp* ferricytochrome *c*′ in ^2H_2O, pH 5.0, at (A) 30 °C and (B) 83 °C (τ_{rec} = 1.12 s) illustrating the loss of structure in the diamagnetic portion of the spectrum.

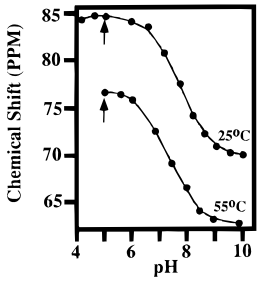

Figure 4. The pH titration curve of peak h_8 of *Rp* ferricytochrome *c*′ (representative of all h_i) at 25 and 55 °C. The sample pH for all NMR spectra (unless otherwise noted) is designated by arrows and occurs in stable portions of the curves for both temperatures.

upfield shifts of −10 ppm and distinctive temperature dependent shifts, h_α, h_β, h_γ, h_δ, x, q; less strongly upfield shifted peaks are considered below. The low-field shoulder of the diamagnetic envelope, moreover, contains, in addition to the apparent methyl peak $h_{2\beta}$, at least three strongly relaxed and low-field-shifted single-proton peaks a, a′, and a″, which can be detected in a series of partially relaxed spectra at 6 °C (supporting information, Figure 6S) for which estimated null points indicate T_1s of 2, 15, and 5 ms and R_{Fe}s of 4.8, 6.6, and 5.8 Å, respectively. The chemical shifts and estimated T_1s for these resonances are listed in Tables 2 and 3.

The Heme. Largely on the basis of extensive NMR studies on model compounds[26] and well-characterized high-spin ferric

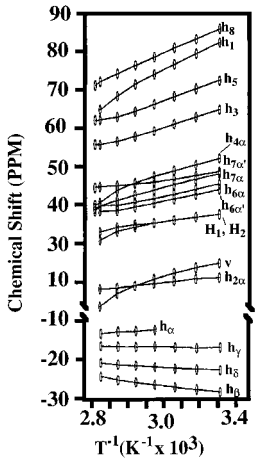

Figure 5. Curie plot (observed shift, δ_{DSS}(obsd), *versus* reciprocal absolute temperature) for the heme and axial His resonances of *Rp* ferricytochrome *c*′, pH 5.0 over the temperature range 20−83 °C illustrating the nonlinear behavior observed for all resonances at elevated temperatures.

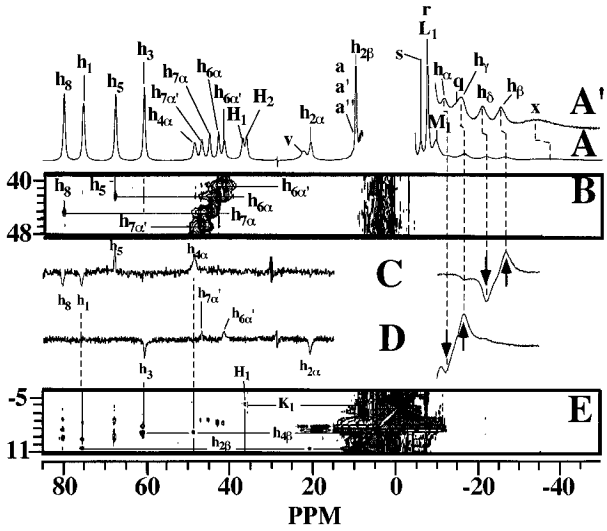

Figure 6. (A) ^{1}H NMR spectra (500 MHz) of *Rp* ferricytochrome *c*′ in ^2H_2O, pH 5.0, at 45 °C (τ_{rec} = 120 ms). (A′) The upfield portion of the NMR WEFT spectrum which more clearly shows peak x; the vertical expansion is approximately 3× that of trace A. (B) Portion of the WEFT-NOESY spectrum (τ_m = 6 ms; τ_{rec} = 86 ms; τ_{rd} = 30 ms) illustrating the cross peaks between downfield-hyperfine-shifted resonances. (C, D) Steady-state NOE difference traces (τ_{rec} = 56 ms) obtained from saturating the resonances (C) h_β minus h_δ and (D) h_γ minus h_α, as shown by vertical arrows. Peaks designated with upright arrows have corresponding upright NOEs; likewise, peaks designated with downward arrows have corresponding downward NOEs. Traces on the left side of the trace label are vertically expanded by 4× relative to those on the right side of the trace label. (E) Portion of the WEFT-NOESY spectrum (τ_{mix} = 6 ms; τ_{rec} = 86 ms; τ_{rd} = 30 ms) at 45 °C illustrating the cross peaks between downfield-hyperfine-shifted resonances and resonances near or in the diamagnetic envelope.

hemoproteins with removable heme,[46,47] the four heme methyls and eight single protons (six H_αs of the heme and the two H_βs of the axial His) are expected in the low-field window 20−100 ppm, and four heme meso-H atoms are expected in the upfield window −10 to −50 ppm for a five-coordinated hemin.[47] In addition to the obvious four low-field methyls, we observe nine

(46) La Mar, G. N.; Budd, D. L.; Smith, K. M.; Langry, K. C. *J. Am. Chem. Soc.* **1980**, *102*, 1822−1827.
(47) Pande, U.; La Mar, G. N.; Lecomte, J. T. J.; Ascoli, F.; Brunori, M.; Smith, K. M.; Pandey, R. K.; Parish, D. W.; Thanabal, V. *Biochemistry* **1986**, *25*, 5638−5646.

strongly low field shifted single proton resonances (Figure 2) and six strongly upfield shifted broad single-proton resonances (Figure 6A). A WEFT-NOESY spectrum with $\tau_m = 6$ ms (Figure 6B) exhibits strong cross peaks within two sets of low-field proton pairs ($h_{7\alpha}/h_{7\alpha'}$ and $h_{6\alpha}/h_{6\alpha'}$) which identify the geminal H_α resonances of the two propionates. Weak cross peaks to two methyl peaks (h_5 and h_8) from one H_α of each propionate identify (but do not differentiate between) the 5-CH_3 and 8-CH_3 peaks. Similar connectivities have been reported for *Cv*[23] and *Rm*[24] ferricytochromes *c*′.

Saturation of four of the six strongly upfield shifted single-proton peaks provides dipolar connectivities to the heme methyls and H_αs, allowing complete assignment of the heme. Saturation of h_δ (Figure 6C; negative peaks) gives NOEs to two methyl peaks (h_1 and h_8), which identify the δ-meso-H and the pair 1-CH_3, 8-CH_3, assigns the 1-CH_3 peak (h_1), and distinguishes between the 5-CH_3 and 8-CH_3 peaks. This also dictates that the remaining methyl peak, h_3, arises from the 3-CH_3. Saturation of h_β (Figure 6C, positive peaks) identifies the β-meso-H resonance by its NOE to the 5-CH_3, and it assigns the 4H_α resonance ($h_{4\alpha}$). Saturation of h_α (Figure 6D, negative peaks) identifies it as α-meso-H by its NOEs to the 3-CH_3 and assigns the 2-H_α resonance, $h_{2\alpha}$. Irradiation of h_γ (Figure 6D; positive peaks) locates the γ-meso-H by its NOEs to both the $H_{6\alpha'}$ and $H_{7\alpha'}$. NOESY cross peaks from the assigned 2-H_α ($h_{2\alpha}$) and 1-CH_3 (h_1) peaks to a relaxed ($T_1 \sim 14$ ms) methyl peak partially resolved on the low-field side of the diamagnetic envelope identifies the 2-$C_\beta H_3$ peak ($h_{2\beta}$), while similar cross peaks from 3-CH_3 and 4-H_α locate the unresolved 4-$C_\beta H_3$ peak $h_{4\beta}$ (Figure 6E). A cross peak from 6-H_αs to a pair of protons near the H_2O signal that are connected by a TOCSY peak locates the 6-H_βs (not shown). A similar peak could not be identified for the 7-H_βs, likely due to the shifts being very close to the H_2O signal. Numerous other NOESY cross peaks between the heme substituents and the diamagnetic envelope are observed in Figure 6E, but are insufficiently resolved for unique analysis; such studies are more effectively pursued by steady-state NOE for the heme (see below).

The strongly relaxed signals H_1, H_2, and v in the low-field window in Figure 2A and q and x in the high-field window in Figure 6A′ must arise from amino acid residues. Saturation of q and x failed to give NOEs to any resolved resonances. The power levels needed to significantly saturate peaks q and x produced sufficient off-resonance effects to the diamagnetic envelope so as to preclude the detection of NOEs to resonances under the diamagnetic envelope.

The Axial His. The two low-field resonances, H_1 and H_2, had been assigned earlier[20] to the axial His 122 H_βs on the basis of comparison to model compounds[26] and other high-spin ferric hemoproteins[46,47] and because of their dramatic downfield shift by ~100 ppm upon conversion to the alkaline form. The increased contact shift for these signals in the alkaline form was shown to be consistent with the proposed[20,25] deprotonation of the axial His. Peak H_1 exhibits a weak NOESY cross peak to signal K_1 (Figure 6E). This unique dipolar connectivity is confirmed by steady-state NOEs over a range of temperatures (not shown). The definitive assignment of peak K_1 to the Lys119 H_α (see below) provides direct evidence for the assignment of H_1 and H_2 to His122 H_βs. The ring protons for His122 are expected to be broadened beyond detection by their proximity to the iron ($R_{Fe} \sim 3.3$ Å, expected $T_1 < 0.1$ ms).

Nonligated Residues with Upfield Dipolar Shifts. The expanded upfield portions of the reference spectrum at 40 °C and pH 5.0 and the WEFT spectrum designed to suppress all peaks with $T_1 > 80$ ms are shown in Figure 7, traces A and B,

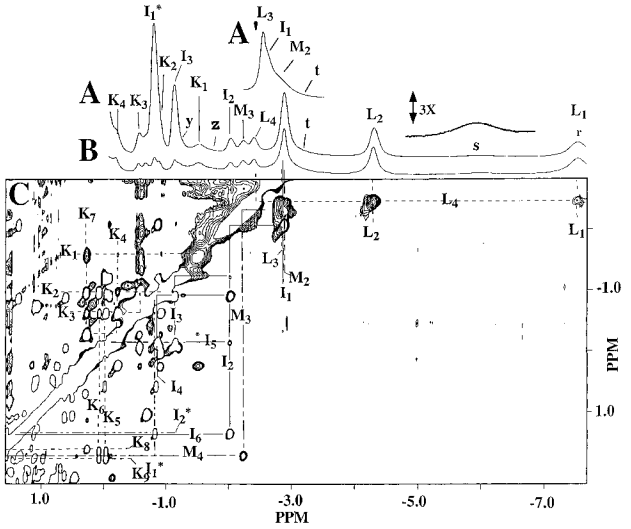

Figure 7. (A) Resolved upfield portion of the 500 MHz ^{1}H NMR spectrum of *Rp* ferricytochrome *c*′ in ^2H_2O, pH 5.0 and at 40 °C ($\tau_{rec} = 3$ s). (B) Resolved upfield portion of the 500 MHz ^{1}H NMR spectrum under saturating conditions ($\tau_{rec} = 200$ ms). (C) Portion of the clean TOCSY ($\tau_m = 8$ ms; $\tau_{rec} = 0.15$ s) spectrum illustrating the cross peaks for the spin systems for resolved upfield resonances.

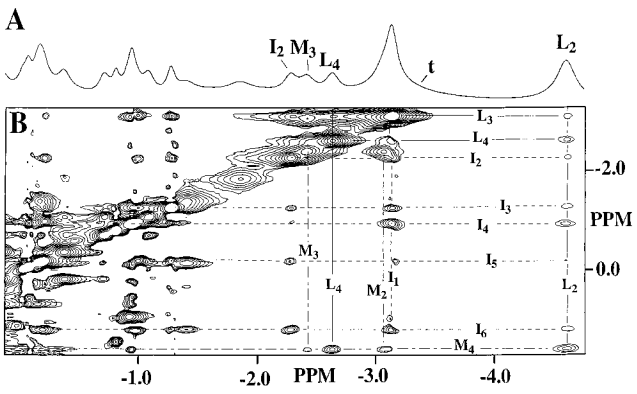

Figure 8. (A) Resolved upfield portion of the 500 MHz ^{1}H NMR WEFT spectrum for *Rp* ferricytochrome *c*′ in ^2H_2O, pH 5.0 and 30 °C ($\tau_{rd} = 40$ ms; $\tau_{rec} = 100$ ms). (B) Portion of the NOESY spectrum ($\tau_m = 15$ ms; $\tau_{rec} = 206$ ms) illustrating the cross peaks between assigned spin systems of resolved upfield resonances.

respectively. Collection of these two types of spectra between 20 and 60 °C locates 19 strongly to moderately relaxed and partially to completely resolved signals (supporting information, Figure 4S). The composite nature of the peak at −3 ppm is better resolved at 60 °C in Figure 7A′. The intercepts at $T = \infty$ in the T^{-1} and T^{-2} plots, $\delta_{int}(T^{-1})$ and $\delta_{int}(T^{-2})$ (given in Table 3), for all non-heme peaks upfield of the diamagnetic envelope (except one resolved peak, I*$_1$; see below) confirm that they experience upfield dipolar shifts.

Two strongly relaxed and resolved methyl peaks L_1 ($T_1 \sim 4$ ms) and L_2 ($T_1 \sim 16$ ms) exhibit TOCSY cross peaks for τ_m of 8 ms (but not 22 ms) to resolved peak L_4, which, in turn, exhibits a TOCSY cross peak to L_3 in the composite at −3.0 ppm (Figure 7C); this identifies a Val or Leu with the two methyls ~5 and 7 Å from the iron. Our homology model has no Val and only one Leu with predicted upfield δ_{dip}, which is also near the heme, Leu16. The 15 ms τ_m NOESY map in Figure 8B shows some of the expected intraresidue cross peaks. Hence we assign the resonances L_i to the $(C_\delta H_3)_2C_\gamma H-C_\beta H$ of Leu16. Two signals confirmed as methyl groups by the retained three-proton intensity over a wide temperature range, I_3 and I_1 ($T_1 \sim 40$ ms), exhibit strong TOCSY connectivities for $\tau_m = 8$ ms (Figure

7C) (but much weaker for $\tau_m = 22$ ms) in a spin system diagnostic for a complete Ile with the $C_\delta H_3$ ≤10 Å from the Fe. The only Ile this close to the iron is Ile15 (Table 1). The upfield portions of the 30 °C WEFT trace and $\tau_m = 15$ ms NOESY map are shown in Figure 8, parts A and B, respectively. In addition to expected intraresidue cross peaks for Ile15, five of its protons exhibit NOESY cross peaks to the Leu16 $C_\delta'H_3$ (L2) (Figure 8B). Leu16 and Ile15 are expected to be in close van der Waals contact, as found for Leu15 and Met16 in *Rm* cytochrome *c*′, providing compelling evidence for these two assignments. The chemical shifts, T_1 values (and resulting R_{Fe}), δ_{dip}(obsd), and intercepts for T^{-1} and T^{-2} plots are collected in Table 3.

The three partially resolved and moderately to strongly relaxed single-proton peaks K_1, K_3, and K_4 exhibit TOCSY cross peaks for $\tau_m = 8$ ms (which are weaker or missing for $\tau_m = 22$ ms) in a pattern that extends into the diamagnetic envelope (with $\tau_m = 22$ ms) to yield a nine-spin system uniquely assigned to a Lys. The TOCSY cross peak topology shows that it is the H_α which is the more strongly shifted (δ_{dip}(obsd) ∼ −5 ppm) and relaxed ($T_1 = 11$ ms, $R_{Fe} = 6.3$ Å) for this Lys and establishes that the backbone, rather than side chain terminus, is oriented toward the iron. Two Lys are near the heme iron, Lys54 and Lys119, and the highly conserved Lys119 on the proximal side of the heme is oriented with its backbone toward the iron. The other Lys54 is a very radical substitution (Ala54 → Lys) in our homology model, but its side chain rather than the backbone would be closer to the iron. The NOESY cross peak from the His122 H_β (peak H_1) to the H_α (K_1) of Lys119 in Figure 6E is precisely what is predicted by the crystal structure of *Rm* and *Cυ* cytochromes *c*′ in this highly conserved portion of the protein, and this result serves to corroborate both the His122 and Lys119 assignments. The pattern of the observed δ_{dip} for Lys119 closely follows that for the predicted δ_{dip} (Table 3). The role of Lys 54 will be considered below.

A strongly relaxed ($T_1 < 1$ ms, $R_{Fe} \sim 4.5$ Å) upfield methyl peak M_1 in Figure 6A exhibits neither TOCSY nor NOESY cross peaks. The only remaining residue in *Rm* cytochrome *c*′ whose substitution would be expected to place a methyl that close to the iron is the $C_\epsilon H_3$ of Met19. Saturation of M_1 yields NOEs to Leu16 H_β, $C_\delta H_3$, as expected for the Met19 methyl (supporting information, Figure 5S). The TOCSY map exhibits cross peaks for two resolved and moderately relaxed single-proton peaks, M_2 and M_3, and one unresolved peak, M_4; we tentatively assign these to part of the side chain of Met19.

A resolved but very weakly relaxed ($T_1 \sim 140$ ms, $R_{Fe} \sim 10$ Å) upfield methyl peak I^*_1 exhibits TOCSY cross peaks to a pair of strongly coupled protons I^*_2 and I^*_3 that uniquely identify an ethyl fragment of an Ile remote from the iron (Figure 7C). Interestingly, both the T^{-1} and T^{-2} intercepts (Table 3) indicate that this methyl experiences a small *low-field* rather high-field dipolar shift in spite of appearing in the high-field side of the diamagnetic envelope. The strongly upfield origin of the methyl dictates that it interact strongly with aromatic residue side chains. Its definitive assignment follows below.

There remain six strongly relaxed ($T_1 \leq 4$ ms, $R_{Fe} \leq 5.5$ Å) and upfield dipolar-shifted single-proton peaks, q, r, s, t, x, and z, which at this time cannot be connected to any other resonance by 1D or 2D methods. The T^{-2} intercepts for peaks q and s (Table 3) indicate aliphatic protons, whereas the intercept for peak x suggests an aromatic side chain origin (see below). Peaks r, t, and u are not sufficiently resolved over the temperature range studied to obtain values for the intercepts. For the residues predicted to exhibit strong upfield dipolar shifts and $R_{Fe} \leq 6$ Å, five signals (Leu16 H_α, H_β, Met19 H_β', Lys126 H_δ, H_δ') are unassigned and hence are candidates for the origins of these peaks. It is also possible that protons on the radical Ala54 → Lys substitution provide candidates for these peaks (see below). The other residues with minor upfield shifts ($\delta_{dip} < 2$ ppm) and weak relaxation ($T_1 \geq 45$ ms, $R_{Fe} > 7.5$ Å), are not assigned; predicted δ_{dip} and R_{Fe} are given in supporting information, Table 2S.

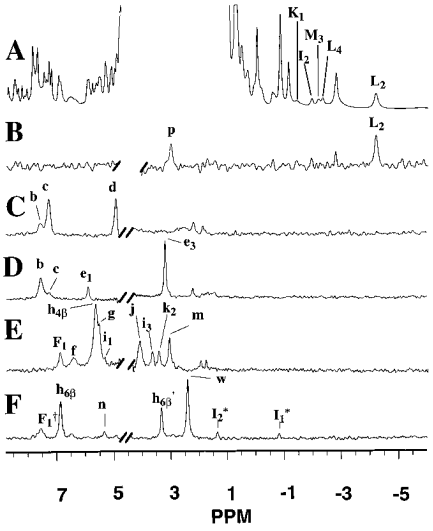

Figure 9. (A) The 8 to −5 ppm region of the 500 MHz ^{1}H NMR spectrum of *Rp* ferricytochrome *c*′ in ^2H_2O, pH 5.0 and 45 °C (τ_{rec} = 3s). Steady-state NOE difference traces obtained from saturating the low-field resonances (B) v; (C) h_1 heme (1-CH_3); (D) h_3 heme (3-CH_3); (E) h_5 heme (5-CH_3); and (F) h_8 heme (8-CH_3).

Nonligated Residues with Low-Field Dipolar Shifts. Residues with predicted sizable (>4 ppm) low-field δ_{dip} are Cys118 H_α ($R_{Fe} = 5$ Å, $\delta_{dip} = 6$ ppm), Cys121 H_β ($R_{Fe} = 7$ Å; $\delta_{dip} = 4$ ppm), H_β' ($R_{Fe} \sim 5$ Å; $\delta_{dip} \sim 6$ ppm), and Lys126 H_γ' ($R_{Fe} = 5$ Å; $\delta_{dip} \sim 4$ ppm) (Table 3). Comparison of δ_{dip} and R_{Fe} suggests the tentative assignment a, a′, a″ to Cys118 H_α, Cys121 H_β, and Cys121 H_β', respectively. Although the distance from Cys121 H_β to 3-CH_3 is ∼3 Å, the strong relaxation renders the expected NOE undetectable (<0.1%).

The NOEs in the unresolved diamagnetic window upon saturating the four heme methyls are shown in Figures 9C−F. The chemical shifts for signals exhibiting NOEs were tracked with temperature and aligned with TOCSY/NOESY maps of the diamagnetic region at the same temperature. The chemical shifts and variable temperature T^{-1}, T^{-2} intercepts for unassigned peaks are provided in the supporting information, Table 1S, and in Table 3 for assigned signals. The common denominator for all of these spatial contacts to the heme periphery is that they exhibit the predicted downfield dipolar shifts, as reflected in the intercepts at $T = \infty$ upfield of the observed position (supporting information, Table 1S). Notable exceptions are NOEs to one peak each from the 3-CH_3 and 5-CH_3 peaks (F_1 and $F_1^\dagger$, respectively), which exhibit little temperature dependence and have intercepts in T^{-1}, T^{-2} plots in the aromatic window, and hence must reflect aromatic rings in contact with the heme (these are considered below). Protons in contact with the heme periphery generally exhibit relatively narrow lines in the NOE difference traces, as might be expected by the Fe ≥ 7 Å dictated by the van der Waals radius in the heme. The 5-CH_3 exhibited an NOE to the H_γ and $C_\delta H_3$ peaks, I^*_2, I^*_1 (Figure 9F), of the Ile $C_\gamma H_2 C_\delta H_3$ fragment identified in the upfield spectrum in Figure 7; this contact uniquely identifies it as Ile74 (see below). Note that Ile74 is correctly predicted to exhibit negligible paramagnetic relaxation and a small low-field dipolar shift, as observed (Table 3). The common NOEs to the heme

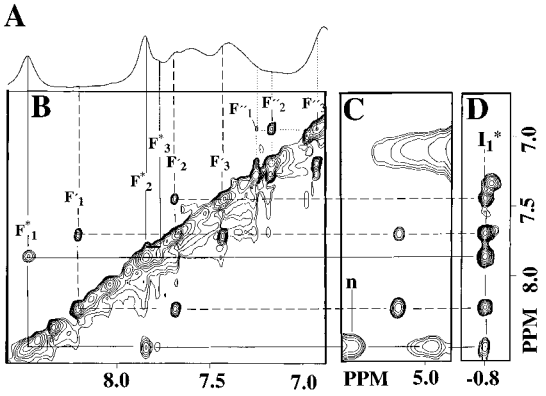

Figure 10. (A) Portion of the aromatic region of the 500 MHz ^{1}H NMR WEFT spectrum *Rp* ferricytochrome *c*′ in ^2H_2O, pH 5.0 and 40 °C (τ_{rd} = 40 ms; τ_{rec} = 100 ms). (B) Portion of the aromatic region of the 500 MHz ^{1}H NMR clean TOCSY spectrum (τ_m = 8 ms; τ_{rec} = 160 ms) in ^2H_2O, pH 5.0 and 40 °C. (C) Portion of the 500 MHz ^{1}H NMR NOESY spectrum (τ_m = 15 ms; τ_{rec} = 2.06 s) in ^2H_2O, pH 5.0 and 40 °C, showing the cross peak which aligns with both F_1* and the 5-CH_3 NOE, peak n. (D) Portion of the 500 MHz ^{1}H NMR NOESY spectrum (τ_m = 150 ms; τ_{rec} = 1.86 s) in D_2O, pH 5.0 at 40 °C, showing the cross peaks from the F_i and F_i′ spin systems to peak I_1*.

1-CH_3 and 8-CH_3 (peaks b and c in Figure 9C,D) are consistent with those predicted for the Gly20 C_αHs ($R_{Fe} \sim 8$ Å, $\delta_{dip} \sim 2-3$ ppm). The $\delta_{int}(T^{-2})$ for peaks b and c is ~4.5 ppm, which is consistent with that expected for H_αs (supporting information, Table 1S). However, in the absence of TOCSY connectivities, these assignments are premature. Other nonaromatic residues with weaker relaxation and small low-field δ_{dip}, Lys13 and Lys17, are not assigned.

The low-field strongly relaxed ($T_1 \sim 3$ ms, $R_{Fe} \sim 5$ Å) peak v exhibits neither TOCSY nor NOESY cross peaks and has no precedence in the spectra of other NMR-characterized[19−25] ferricytochromes *c*′. Hence this peak must reflect a very nonconservative substitution near the heme. The most likely candidate for such a substitution relative to *Rm* cytochrome *c*′ that can bring a proton to within 5 Å in *Rp* is Ala54 → Lys, which occurs in the distal peptide region connecting helix 2 and helix 3. The crystal structures of *Rm*[12,13] and *Cv*[11] cytochrome *c*′ show that this region of the protein adopts variable positions relative to the heme iron for both the side chains and backbone. The δ_{dip}(calcd) therefore can range from large upfield to large downfield, depending on the Lys54 orientation. Saturation of peak v yields an NOE to Leu15 peak L_2, as shown in Figure 9B, which confirms the distal origin of the residue. If Lys54 is responsible for peak v, other side chain protons must also be close to the iron.

Aromatic Residues. Side chain protons of aromatic residues can be identified either by their temperature independent shifts in the characteristic aromatic window 6−8 ppm or by intercepts in this window for the T^{-1}, T^{-2} plots. Two of the six aromatic residues, Phe36 and Trp75, are expected to be remote from the heme (>15 Å). Two, Phe58 and Phe86, are expected to make contact with the heme 5-CH_3 and 3-CH_3, respectively, but are also expected to exhibit significant relaxation and/or dipolar shifts for some of the ring protons (Table 3). Lastly, Phe58, Phe82, and Phe125 are expected to interact with the Ile74 side chain in the highly conserved hydrophobic core.

The TOCSY spectrum of the aromatic window is shown in Figure 10B, along with the WEFT reference trace in Figure 10A. Three complete Phe rings are identified, F′, F″, and F*, of which two, F′ and F″, show insignificant hyperfine shifts, and their resonances are completely suppressed in the WEFT trace in Figure 10A. The third complete ring, F*, exhibits significant downfield shifts for F_1* and experiences strong paramagnetic relaxation as witnessed by the retained intensity of F_1* (and also F_2*) in the WEFT trace in Figure 10A, and by the observation of stronger F_1*−F_2* NOESY cross peaks in the τ_m = 15 ms than in the τ_m = 50 ms NOESY map. F_1* does not exhibit NOEs to the heme, but exhibits a NOESY cross peak to the Ile74 $C_\delta H_3$ (Figure 10D) and a shared contact (peak n) with the heme 5-CH_3 (Figure 10C), which identifies F* as arising from Phe82 and confirms the Ile74 assignment. The weak low-field dipolar shifts are consistent with the expectations for Phe82 (Table 3). The steady-state NOEs from 3-CH_3 to F_1 and 5-CH_3 to F_1† are those expected for Phe86 and Phe58, respectively. The analogs of both residues in *Rm* cytochrome *c*′ indicate that the remaining ring protons could be strongly relaxed but only moderately dipolar shifted (see below) (Table 3), which likely accounts for the failure to detect other ring protons by TOCSY. These two side chains are close to the magic angle ($\theta \sim 54°$ in eq 4), making predictions of δ_{dip} unreliable.

It is noted that none of the *Rp* protons are predicted by our homology model to exhibit the large δ_{dip} that could give rise to peak x at −38 ppm. However, if δ_{dip} is calculated *directly* for Trp86 in the *Rm* cytochrome *c*′ crystal structure, the Trp86 H_6 has $R_{Fe} \sim 3.8$ Å and $\delta_{dip} = -30$ ppm for $D = 12$ cm^{-1}. The substitution Trp86 → Phe in our homology model for *Rp* necessarily places the phenyl group in *Rp* further from the iron than the Trp in *Rm* cytochrome *c*′. However, if the helix moves toward the heme to allow van der Waals contact between the heme and Phe86 in the manner found for Trp86 in *Rm* cytochrome *c*′, a similarly large upfield δ_{dip} can be expected for Phe86; note that the intercept with the T^{-2} plot also suggests an aromatic proton as the origin of peak x (Table 3). Hence we suggest the tentative assignment for peak x as H_4 of Phe86.

Since none of the ring protons of Phe F′ exhibit significant relaxation and/or shifts and all show contact to the Ile74 $C_\delta H_3$ (Figure 10D), the origin of F_i′ must be Phe125. The remaining Phe F″$_i$ is distant from the heme and not in contact with Ile74 and must arise from Phe36. Trp75, which is expected to be far from the heme, was not identified in the TOCSY map, possibly because of near degeneracy of the ring peaks. The large number of low-field dipolar-shifted aliphatic protons which resonate in the aromatic window (see Figure 10A) precluded a search for Trp based on peak intensity.

Discussion

Assignment/Structure Determination Strategy. 2D/1D NOE data provided the complete assignment of heme core substituents in a fashion similar to that used for diamagnetic ferrocytochromes[48] *b* and *c*. The only limitation to extending this approach to other hemoproteins is that the meso-H resonances must be resolved in the upfield spectral window. In spite of the large line widths and short T_1s for resonances close to the heme, the increased dispersion due to δ_{dip} for noncoordinated residues allows detection of the majority of the protons with expected $T_1 \leq 50$ ms. More surprisingly, TOCSY allowed detection of sufficient scalar connectivities even for peaks with $T_1 \sim 4$ ms (L_1) to uniquely identify the residue type, which, with dipolar connectivities to the heme, axial His and/or other residues, in conjunction with the sequence homology to structurally characterized cytochromes *c*′, allow unique assignments for Ile15, Leu16, and Met19 in the distal pocket, and Lys119 and His122 on the proximal side of the heme. It is

(48) Keller, R. M.; Wüthrich, K. *Biochim. Biophys. Acta* **1980**, *621*, 204−217.

noted that, while we cannot offer even tentative individual assignments for the five resolved strongly relaxed and upfield-dipolar-shifted single-proton peaks q, r, s, t, and z (bottom of Table 3), the range of T_1s and δ_{dip} (when available) correlate with values expected for the unassigned signals, Leu H_β, H_α, Met19 H_β', Lys126 H_δ, H_δ', in Table 3. The strongly relaxed and shifted signals from the Cys118 and Cys121 cannot be definitively assigned, but resonances consistent with the predicted relaxation and low-field dipolar shifts are detected. It is noted here that the side chains of the residues detected and characterized in this study are included among those which were not detected[18] in the 2D NMR study of *Rc* ferricytochrome *c*′.

The definitive assignments of the heme, axial His, several distal pocket residues, and Ile74 (which interacts with several aromatic side chains) provide one element of independent confirmation of the structural homology of the monomeric *Rp* cytochrome *c*′ to the subunits of the structurally characterized[11−15,18] cytochromes *c*′. The correlation between observed and predicted δ_{dip} *direction* is excellent; the correlation between observed and predicted δ_{dip} *magnitude* is surprisingly good in view of the crudeness of the homology model. It is noted that the predictions are best for the structurally conserved and definitively assigned residue Lys119 (Table 3). These data therefore provide additional support for strong structural homology for *Rp* to other structurally characterized ferricytochromes *c*′. The qualitative correlation between observed and predicted δ_{dip} show that these shifts will serve as valuable constraints in developing a molecular model of cytochrome *c*′ as established for low-spin ferric hemoproteins.[32−34,36]

There are several strongly relaxed proton resonances which cannot be assigned by the present method, but whose relaxation and dipolar shift properties are consistent with a number of unassigned protons. However, it is expected that ^{13}C and ^{15}N labeling would provide the route to identifying even these protons.[18] The ^{13}C and ^{15}N near the heme are much less influenced by paramagnetic relaxation because of their relative magnetogyric ratios, allowing the detection of $^1H-^{13}C$ and $^1H-^{15}N$ heteronuclear correlation to the broad ^1H signal.[49,50] Moreover, while NOESY connectivities among strongly relaxed protons may be lost, the use of the ^1H and ^{15}N δ_{dip} and relative T_1s provides the necessary constraints to make a complete solution structure determination of a ferricytochrome *c*′ a good prospect.

Heme Electronic/Molecular Structure. The NOE connectivities around the heme periphery, as detected by a combination of 2D and 1D experiments, provide all of the pyrrole-α and meso-H assignments and confirm that the meso-H signals indeed resonate upfield, as expected for a five-coordinate high-spin iron(III) heme.[26,47,51] On the other hand, there are six upfield peaks with relaxation/shift properties reflective of meso-H. This dictates that simply observing upfield signals is not sufficient to assign the ligation/spin state; the meso-H signals must be identified by their characteristic proximity to the appropriate low-field pyrrole substituent(s). The present complete heme assignments for *Rp* ferricytochrome *c*′ are consistent with partial assignments for *Cv* and *Rc* .[23,24]

The intercepts at $T = \infty$ for δ_{DSS}(obsd) versus T^{-2} (but not T^{-1}) plots for all nonligated residue protons are characteristic of the expected δ_{dia} for the various functional groups (methyls, ~1 ppm; H_β ~2−3 ppm; H_α, ~4.5 ppm; aromatic, ~7 ppm; see Table 3), which indicates that a single high-spin ferric ion with a fixed *D* value can account for the dipolar shifts for the nonligated residues. The six-coordinate high-spin ferric heme in metMbH_2O[44,45] exhibits $D \sim 8$ cm^{-1}, and comparison of the dipolar shift in the WT protein and a mutant that abolishes the ligated water shows an increase in *D* of a factor of 1.5−2 in the five-coordinate mutant.[51] Hence $D = 12$ cm^{-1} is a reasonable estimate for the five-coordinate high-spin ferricytochrome *c*′. It is possible, however, to independently determine *D* by EPR.[44] The heme methyl shifts more closely follow the T^{-1} behavior predicted for the contact shifts (eq 2), which is consistent with only small ($\delta_{dip} \sim 8$ ppm) dipolar contribution of the same sign relative to the much larger contact shifts. The meso-H atoms, on the other hand, exhibit a range of deviations from the T^{-1} lines. However, the $D \sim 12$ cm^{-1} predicts large (+18 ppm) low-field dipolar shifts for meso-H atoms, which are comparable in magnitude, *but opposite in sign*, to the upfield contact shifts which will lead to large deviations for the Curie law in the manner observed.

The NOE connectivities around the heme confirm a geometry for the thioether linkages that is the same as that generally found for other cytochromes *c*′, with the 2-H_α oriented toward the α-meso-H, the 2-$C_\beta H_3$ toward the 1-CH_3, the 4-H_α toward the β-meso-H, and the 4-$C_\beta H_3$ toward the 3-CH_3, as shown in Figure 1. The larger δ_{DSS}(obsd), and hence δ_{con}, for the 1-CH_3 than 3-CH_3 indicates that more spin density is delocalized to pyrrole A than B. The much larger 4-H_α than 2-H_α shifts, therefore, must reflect slightly different orientations of the thioether linkage. The relevant dihedral angles in eq 3 for the 4-H_α and 2-H_α are ~40° and ~25°, respectively, which yields a predicted $\delta_{con}(4H_\alpha)/\delta_{con}(2H_\alpha)$ of ~1.6 and in part rationalizes the larger 4-H_α than 2-H_α shift. The very similar δ_{DSS}(obsd) for the H_αs for both the 6- and 7-propionate indicates extended chains, which is consistent with the crystal structure.

Thermal Unfolding and Intermediates. The loss of all dispersion in the diamagnetic portion of the NMR spectrum at higher temperatures (Figure 3B) indicates that the protein has unfolded with a melting temperature of ~78 °C. The process is completely reversible even at high (~5 mM) concentration. The detection of three peaks, u_1, u_2, and u_3, consistent with the chemical shifts and relative intensities expected for heme methyl protons (12), pyrrole H_αs (6), and meso-H atoms (4) reflects approximately four-fold symmetry and suggests that the axial His bond is lost in the unfolded state. A similar unfolding is observed for the alkaline form at slightly lower temperature, although the unfolded form appears to contain a low-spin ferric heme (see supporting information).

The ^1H NMR spectra in Figure 2 and the Curie plot in Figure 5 show that the folded protein with peaks h_i exhibits changes in structure at temperatures below where unfolding occurs; the changes are in the form of changed slopes in the Curie plots near 70 °C for 1-CH_3 (Figure 5), as well as other single-proton peaks, and a dramatic increase in the 1-CH_3 peak line width (Figure 2B,C), when compared with the 3-CH_3 or 5-CH_3 peaks. These spectral changes indicate equilibrium structural change(s) prior to unfolding. The unchanged T_1 values for 1-CH_3 relative to the other methyls at elevated temperature dictate that the broadening results from an exchange effect,[52] *i.e.*, the 1-CH_3 senses the average of two or more different equilibrium

(49) Bertini, I.; Luchinat, C.; Macinai, R.; Piccioli, M.; Scozzafava, A.; Viezzoli, M. S. *J. Magn. Reson.* **1994**, *B104*, 95−98.
(50) Sadek, M.; Scrofani, S. D. B.; Brownlee, R. T.; Wedd, A. G. *J. Chem. Soc., Chem. Commun.* **1995**, *1*, 105−108.
(51) Rajarathnam, K.; La Mar, G. N.; Chiu, M. L.; Sligar, S. G.; Singh, J. P.; Smith, K. M. *J. Am. Chem. Soc.* **1991**, *113*, 7886−7892.
(52) Sandström, J. *Dynamic NMR Spectroscopy*; Academic Press: New York, 1982; pp 14−18.

environments whose influence is localized near pyrrole A (Figure 1).

The unfolding of the four-helical-bundle proteins has been proposed[53] to be initiated by the separation of two pairs of helices, *i.e.*, the first and second helices from the third and fourth. The ferricytochrome *c*′ heme is covalently attached to helix 4 and makes the most contacts (via pyrroles B and C) with residues on helices 3 and 4. Helix 2 does not have contacts with the heme. Helix 1 makes contacts with pyrroles A and D, which possess the 1-CH_3 and 8-CH_3, with pyrrole A further from the helix hinge and, hence, more likely to sense a perturbation of helices 1 and 2. Thus, the line width perturbation of the 1-CH_3 resonance at elevated temperature is consistent with exchange between the completely folded protein and an equilibrium intermediate that has an altered interaction between the heme and helix 1 and is consistent with, but not proof for, the "peeling" away of helices 1 and 2 from 3 and 4. The NOEs from the heme 1-CH_3 to peaks e_1 and e_3 show decreased intensity relative to the NOE to the 2-$C_\beta H_3$ ($h_{2\beta}$) at 60 °C when compared to 30 °C (not shown), which is consistent with population of some species having perturbed contact with the helix near 1-CH_3. More detailed interpretation of the structural perturbations will require much more extensive assignments of the "diamagnetic" portion of the protein over a range of temperatures, possibly with ^{15}N labeling, and is beyond the scope of this study.

(53) Kobayashi, Y.; Sasabe, H.; Saitô, N. *J. Protein Chem.* **1993**, *12*, 121−131.

Acknowledgment. The authors are indebted to Dr. J. S. de Ropp for experimental assistance and to the National Institutes of Health (HL-16087, GM-21277) and National Science Foundation (DMB91-04018) for support of this research.

Supporting Information Available: Tables of observed spectral parameters for unassigned resonances, predicted spectral parameters for nonligated resonances, and spectral parameters for heme and axial His at pH 10, 40 °C), and figures depicting the effect of temperature on hyperfine-shifted resonances at pH 10, the effect of temperature on the diamagnetic envelope at pH 10, the effect of temperature on strongly upfield shifted resolved resonances at pH 5, the effect of temperature on moderately upfield shifted resolved resonances at pH 5, the steady state NOE of Met19 $C_\epsilon H_3$ at pH 5, and partially relaxed spectra to resolved four strongly relaxed resonances near 12 ppm at pH 5 (9 pages). This material is contained in libraries on microfiche, immediately follows this article in the microfilm version of the journal, can be ordered from the ACS, and can be downloaded from the Internet; see any current masthead page for ordering information and Internet access instructions.

JA953719T